

Delineation and Quantification of Wetland Depressions in the Prairie Pothole Region of North Dakota

Qiusheng Wu & Charles R. Lane

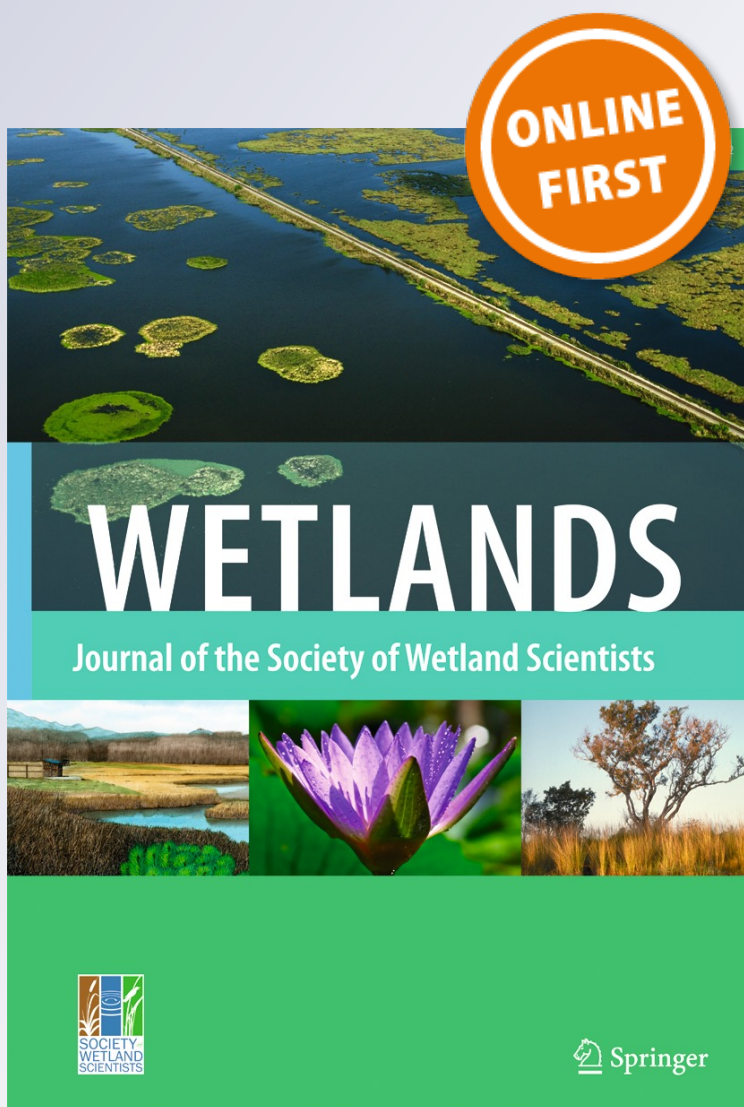
Wetlands

Official Scholarly Journal of the Society
of Wetland Scientists

ISSN 0277-5212

Wetlands

DOI 10.1007/s13157-015-0731-6



 Springer

 Springer

Your article is protected by copyright and all rights are held exclusively by Society of Wetland Scientists. This e-offprint is for personal use only and shall not be self-archived in electronic repositories. If you wish to self-archive your article, please use the accepted manuscript version for posting on your own website. You may further deposit the accepted manuscript version in any repository, provided it is only made publicly available 12 months after official publication or later and provided acknowledgement is given to the original source of publication and a link is inserted to the published article on Springer's website. The link must be accompanied by the following text: "The final publication is available at link.springer.com".



Delineation and Quantification of Wetland Depressions in the Prairie Pothole Region of North Dakota

Qiusheng Wu^{1,3}  · Charles R. Lane²Received: 12 August 2015 / Accepted: 27 December 2015
© Society of Wetland Scientists 2016

Abstract The Prairie Pothole Region of North America is characterized by numerous, small, wetland depressions that perform important ecological and hydrological functions. Recent studies have shown that total wetland area in the region is decreasing due to cumulative impacts related to natural and anthropogenic changes. The impact of wetland losses on landscape hydrology is an active area of research and management. Various spatially distributed hydrologic models have been developed to simulate effects of wetland depression storage on peak river flows, frequently using dated geospatial wetland inventories. We describe an innovative method for identifying wetland depressions and quantifying their nested hierarchical bathymetric/topographic structure using high-resolution light detection and ranging (LiDAR) data. This contour tree method allows identified wetland depressions to be quantified based on their dynamic filling-spilling-merging hydrological processes. In addition, wetland depression properties, such as surface area, maximum depth, mean depth, storage volume, etc., can be computed for each component of a depression as well as the compound depression. We successfully applied the proposed method to map wetland

depressions in the Little Pipestem Creek watershed in North Dakota. The methods described in this study will provide more realistic and higher resolution data layers for hydrologic modeling and other studies requiring characterization of simple and complex wetland depressions, and help prioritize conservation planning efforts for wetland resources.

Keywords Wetland hydrology · Topographic depressions · Water storage · LiDAR · Prairie Pothole Region · Geographically isolated wetland · Non-adjacent wetland

Introduction

The Prairie Pothole Region (PPR) of North America encompasses an area of approximately 715,000 km², including portions of Canada and the state of Minnesota, Iowa, North Dakota, South Dakota, and Montana in the U.S. (Fig. 1). The PPR is characterized by millions of wetland depressions created by the last glacial retreat more than 10,000 years ago (Winter 1989). These wetland depressions (or “potholes”) are typically small and shallow, with an estimated median size of 1,600 m² and depths generally less than one meter (Huang et al. 2011a). They vary in ponded water permanency, expressing ephemeral, temporal, seasonal, semi-permanent, and permanent hydroperiods, depending on precipitation patterns, soil conditions, and contributing area (Sloan 1972). These depressional potholes have the capability to retain a considerable amount of water which may or may not be released to contribute to overland flow. Extent and distribution of these depressions as well as antecedent water stored within them control the area contributing to the basin outlet (Ehsanzadeh et al. 2012). The water supplied to potholes is largely from direct precipitation, surface inflows from upland, and near-surface groundwater seepage (Todhunter and

✉ Qiusheng Wu
wqs@binghamton.edu; Wu.Qiusheng@epa.gov

Charles R. Lane
Lane.Charles@epa.gov

¹ Department of Geography, State University of New York, Binghamton University, Binghamton, NY 13902, USA

² Office of Research and Development, U.S. Environmental Protection Agency, 26 W. Martin Luther King Dr., Cincinnati, OH 45268, USA

³ CSS-Dynamac c/o U.S. Environmental Protection Agency, 26 W. Martin Luther King Dr., Cincinnati, OH 45268, USA

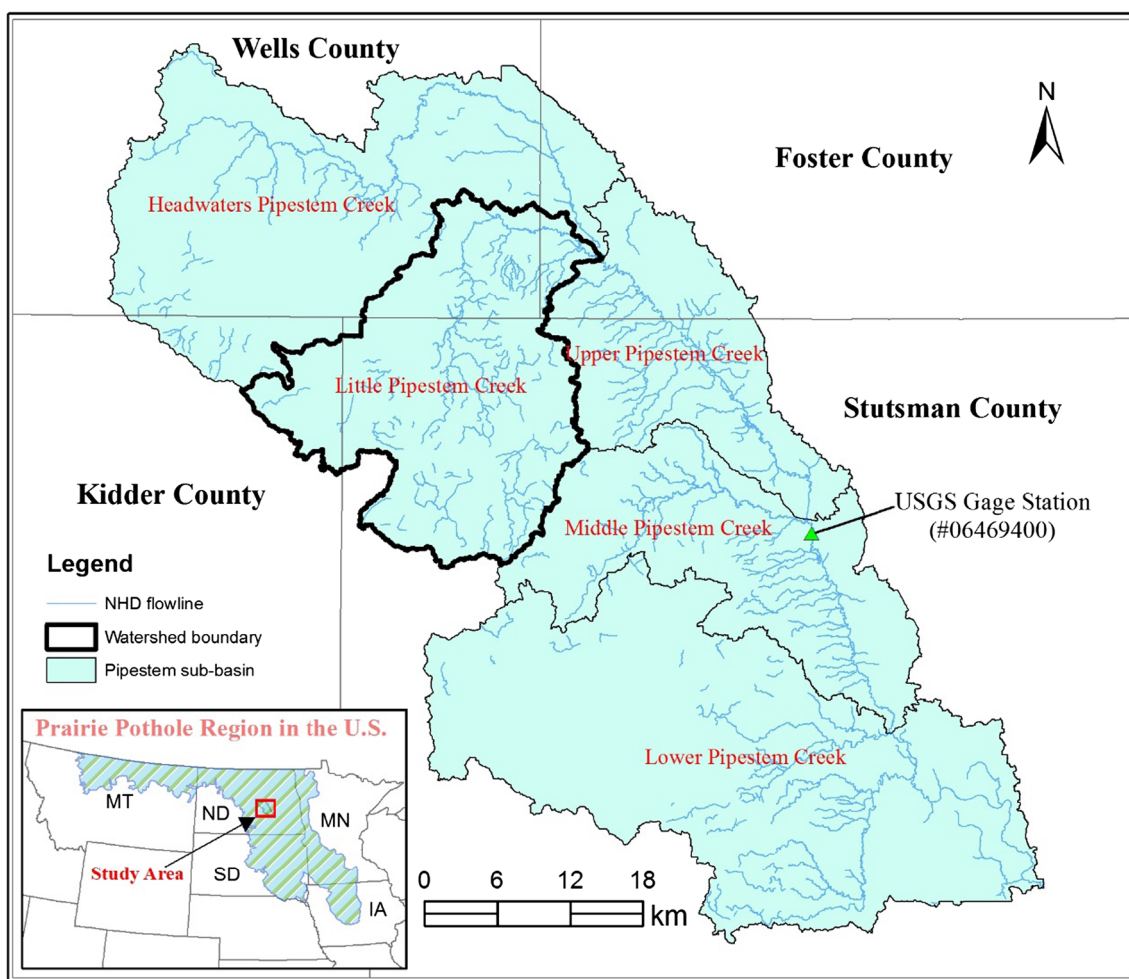


Fig. 1 Location of the Little Pipestem Creek watershed in North Dakota

Rundquist 2004). Water losses from potholes are primarily driven by evapotranspiration (ET) during summer, with net ET typically exceeding net precipitation during the growing season. Since depressional potholes are relatively small in size, shallow in depth, and dependent largely on precipitation and ET, most are ephemeral (Winter and Rosenberry 1995). As a result, depressional potholes in the PPR are especially sensitive to natural climatic variability, human-induced climate change, and human modification of land-surface hydrology (e.g., ditches and draining), making them one of the most dynamic hydrological systems in the world (Todhunter and Rundquist 2004). However, they are also vulnerable systems, in part due to their hydrology.

Dahl (1990) estimated that the lower 48 states in the U.S. lost an approximate 53 % of their original wetland area between the 1780s and the 1980s. The latest report on the status and trends of prairie wetlands (Dahl 2014) estimated that total wetland area declined by 301 km² or 1.1 % in the PPR between 1997 and 2009, primarily driven by cumulative impacts from altered hydrology and associated anthropogenic changes

such as draining, ditching or filling of depressions. The extensive alteration and reduction of wetland depressions have been found to be partially related to the increasing magnitude and frequency of flood events along rivers in the PPR (Miller and Nudds 1996; Gleason et al. 2007; Ehsanzadeh et al. 2012; Johnston 2013; Townsend-Small et al. 2013; McCauley and Anteau 2014).

In the past decades, numerous wetland hydrology studies have been undertaken in the PPR (Sloan 1972; Winter and Rosenberry 1995; Lindsay 2004; Gleason et al. 2007; Johnson et al. 2008; Huang et al. 2011b; Johnston 2013; Shaw et al. 2013; Ouyang et al. 2014). Depression storage is a dominating storage element in the PPR, as well as other areas of the U.S. (e.g., Lane and D'Amico 2010), where it accounts for most of the retention on a watershed surface (Ullah and Dickinson 1979a). While several researchers have focused on identifying topographic depressions for hydrologic modeling and wetland studies, we have found no studies quantifying depression storage hierarchy in potholes resulting from changing water levels within these systems. This lack of

fine-scale detail can create errors within hydrological models when models do not account for intra-depression hierarchical hydrodynamics.

Before the advent of digital elevation models (DEMs), the values of depression storage were usually assumed or indirectly estimated due to practical difficulties in making direct measurement of the basin morphology of individual depression (e.g., Haag et al. 2005). With increasing availability of high-resolution DEMs derived from light detection and ranging (LiDAR) data, depression storage can now be accurately measured, as LiDAR-derived DEMs are often capable of representing actual depressions in the landscape because of their fine scale and high horizontal and vertical accuracies (Wu et al. 2014, 2016). The traditional approaches to identifying surface depressions assume that overland flow initiates after all surface depressions are fully filled. In reality, surface depressions may be filled gradually due to different input conditions, which results in a dynamic filling, spilling, and merging of intra-depression topographic features affecting hydrological processes (Yang and Chu 2013).

In this study, we propose a localized contour tree method to identify pothole depressions and characterize their nested hierarchical structure based on a high-resolution LiDAR DEM. The unique features of this innovative depression delineation and characterization algorithm include: (1) accounting for dynamic filling, spilling, and merging hydrologic processes that are not considered in current depression identification algorithms; (2) representing and visualizing topological relationships between depressions using the contour tree graph, clearly showing the nested hierarchical structure of depression complexes; and (3) characterizing depression geometric properties (e.g., maximum and average depth, perimeter, surface area, and depression storage, etc.). These features provide important and improved inputs for hydrologic modeling and watershed management.

Study Area

The Little Pipestem Creek watershed study area is located within the 2,770 km² Pipestem River sub-basin, which is part of the Missouri River Region – James River Sub-Region. The Little Pipestem Creek watershed is a 10-digit (#1016000202) Hydrologic Unit Code (HUC) system with an approximate area of 506 km², covering parts of four counties (Foster, Kidder, Stutsman, and Wells) in North Dakota (see Fig. 1). Land-use and land-cover data (Table 1) derived from the National Land Cover Database 2011 (Jin et al. 2013) characterizes the watershed as dominated by Herbaceous (35.9 %) and Cultivated Crops (35.1 %), with considerable amounts of Open Water (9.4 %) and Emergent Herbaceous Wetlands (5.9 %). The area is further characterized by a temperate and humid climate with an average annual precipitation of 40 cm.

Table 1 Land-use / land-cover composition of the Little Pipestem Creek watershed, North Dakota

Land-cover type	Area (km ²)	Percentage
Open water	47.8	9.4 %
Developed, open space	15.8	3.1 %
Deciduous forest	1.3	0.2 %
Herbaceous	181.9	35.9 %
Hay/Pasture	51.5	10.2 %
Cultivated crops	178.1	35.1 %
Woody wetlands	0.7	0.1 %
Emergent Herbaceous wetlands	29.6	5.9 %
Total	506.6	100.0 %

(Data source: National Land Cover Database 2011)

The landscape is hummocky and contains numerous closed wetland depressions. Most wetlands are inundated or saturated for a relatively short period in the spring following snowmelt. The period of maximum water depth varies with inter-annual fluctuations in weather conditions, but typically takes place in March and April when evapotranspiration remains relatively low but basins are receiving snowmelt inputs. Stream flows are typically highest during February through April (Shook and Pomeroy 2012), as a result of snowmelt.

Datasets

Several high-resolution remotely sensed data sets were used in our study, including the bare-earth LiDAR DEM, LiDAR intensity imagery, color-infrared aerial photographs, and National Wetlands Inventory (NWI) maps (Table 2).

LiDAR-Derived Bare-Earth DEM

The LiDAR data for our study area were collected with a Leica sensor ALS60 from October 27, 2011 to November 3, 2011 as part of the James River Basin LiDAR acquisition campaign, a collaborative effort among the US Army Corps of Engineers, US Fish and Wildlife Service, Natural Resources Conservation Service, and North Dakota State Water Commission. The LiDAR-derived bare-earth DEMs were distributed through the North Dakota LiDAR Dissemination Service (<http://lidar.swc.nd.gov/>, accessed December 16, 2014) as 2,000 m × 2,000 m tiles with 1-m pixel resolution. The LiDAR DEM was in the Universal Transverse Mercator (UTM) Zone 14 N map projection referenced to NAD83 and NAVD88 horizontal and vertical datums. The overall vertical accuracy assessment at the 95 % confidence level of the LiDAR DEM was reported to be 15.0 cm on open terrain. The Little Pipestem Creek watershed study area

Table 2 Summary of data sets acquired, data acquisition dates, data resolution, and use

Data set	Acquisition dates	Resolution	Application
LiDAR DEM	10/27/2011–11/3/2011	1 m	deriving depressions
LiDAR intensity	10/27/2011–11/3/2011	1 m	deriving waterbodies
Aerial photographs	7/14/2012–7/30/2012	1 m	validating depressions
National wetlands inventory	1979–1984	1:24 K (~12.5 m)	comparing results

was composed of 164 DEM tiles. The Dynamic Raster Mosaicking function in ArcGIS (ESRI, Redlands, CA, version 10.2) was used to create a mosaicked dataset that combined the 164 DEM tiles as a seamless 1-m raster for all subsequent image analyses and map generation. The shaded relief map of the LiDAR-derived bare-earth DEM with National Hydrography Dataset (NHD) flowlines overlaid on top is shown in Fig. 2a. The elevation of the watershed ranges from 471 to 651 m, with relatively high terrain in the south and low terrain in the north. Streams and rivers flow northwards and merge into the Pipestem Creek (see NHD flowlines in Fig. 2a).

It should be noted that the reliability of LiDAR-based geometric properties of wetland depressions, particularly water surface area and storage volume, are affected by antecedent water storage and dense vegetation. The LiDAR data were acquired during leaf-off conditions, with no measurable precipitation for the week prior to the LiDAR campaign (NOAA National Climate Data Center, <http://www.ncdc.noaa.gov/>, accessed December 16, 2014), though we did not conduct field-based inspections of surface hydrology.

LiDAR Intensity Imagery

LiDAR intensity data were simultaneously collected with the LiDAR elevation point clouds during the acquisition campaign. The intensity is a measure of the return signal strength of the laser pulse that generated the point, which is largely determined by the reflectivity of materials within the light path. Intensity data can be used to identify different types of materials on the ground, especially when those features have distinct reflectances in the partition of the electromagnetic spectrum detected by the sensor (Lang and McCarty 2009). Since most topographic LiDAR sensors operate in the near-infrared wavelengths, which tend to be absorbed by water, the return amplitude from water is typically very weak. As a result, waterbodies tend to be characterized as very dark features in the LiDAR intensity image (Fig. 2b). The intensity value ranges for the LiDAR intensity imagery in our study area ranged from 0 to 248. The LiDAR intensity data were primarily used for identifying existing waterbodies in the study area, though it can also serve as a substitute for aerial imagery when none is available to validate wetland depressions delineated from LiDAR DEMs.

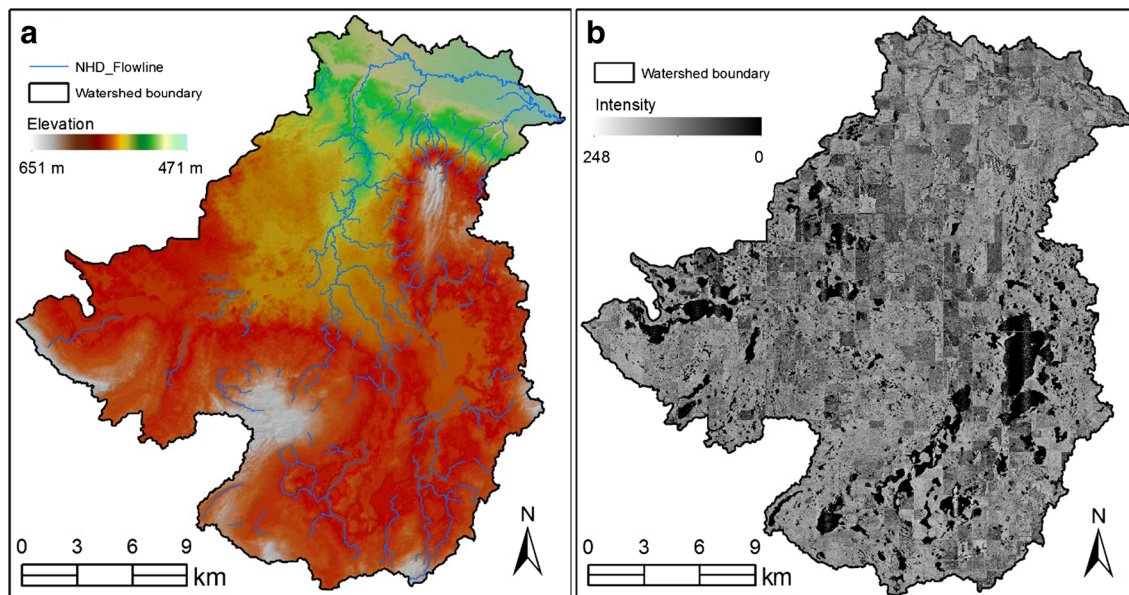


Fig. 2 LiDAR data for the Little Pipestem Creek watershed: **a** shaded relief map of the LiDAR-derived bare-earth DEM (2011); **b** LiDAR intensity imagery (2011)

Aerial Photographs

Cloud-free four-band (red, green, blue, and near-infrared) aerial photographs for the study area were collected from July 14, 2012 to July 30, 2012 by the U.S. Department of Agriculture's National Agriculture Imagery Program (NAIP) during the agricultural growing season. The data can be obtained from the North Dakota GIS Hub Data Portal (<http://www.nd.gov/gis/>, accessed December 16, 2014). The tiling format of the NAIP imagery is based on a $3.75' \times 3.75'$ quarter quadrangle with a 300 pixel buffer on all four sides. Our study area was comprised of 29 tiles, which were mosaicked together and clipped to the watershed boundary to create a seamless raster image (Fig. 3a). The color-infrared (CIR) aerial photographs were used for visual assessment of wetland depressions detected from the LiDAR DEM. It should be noted that the aerial photographs were acquired in summer 2012, when water levels were lower and water surface areas were smaller than those in fall 2011 when the LiDAR data were acquired, as evidenced by visual comparisons of existing water areas between the LiDAR intensity imagery and aerial photographs (see below).

National Wetlands Inventory Data

We used NWI data (<http://www.fws.gov/wetlands/>, accessed December 16, 2014) for our study area for validation and results comparison. These data were derived by manually interpreting aerial photographs acquired from 1979 to 1984 at a scale of 1:24,000 with subsequent support from soil surveys and field verification. Wetlands were classified

based on dominant vegetation structure into various types (see Table 3). More information about wetland classification systems can be found in Cowardin et al. (1979). National Wetlands Inventory maps have a targeted mapping unit, which is an estimate of the minimum sized wetland that can be reliably mapped (Tiner 1997); it is not the smallest wetland that appears on the map. The targeted mapping unit for the PPR was 0.1 to 0.4 ha (Tiner 1997; Johnston 2013). There were 8,091 NWI polygons across the Little Pipestem Creek watershed, including palustrine, lacustrine, and riverine systems. Freshwater (palustrine) emergent wetland was the dominant wetland type, with 7,804 wetland polygons accounting for 84 % of the total wetland area in the study area. Of the 225 freshwater pond polygons, 124 of them were nested within freshwater emergent wetland polygons. Each part of wetland polygons composed of multiple parts were assessed individually, namely each part was considered a unique polygon in our study. The total area of all NWI polygons was approximately 62 km^2 , covering 12.3 % of the watershed area (506 km^2).

It should be noted that the NWI data in this region are considerably out of date, as they were manually interpreted from black and white aerial photographs that were acquired more than 20 years ago. NWI data is a static dataset that does not reflect wetland temporal change (Euliss et al. 2004; Huang et al. 2011b), and the positional accuracy associated with the wetland polygons is largely unknown. However, the NWI data does provide a valuable source for wetland location information (Tiner 1997).

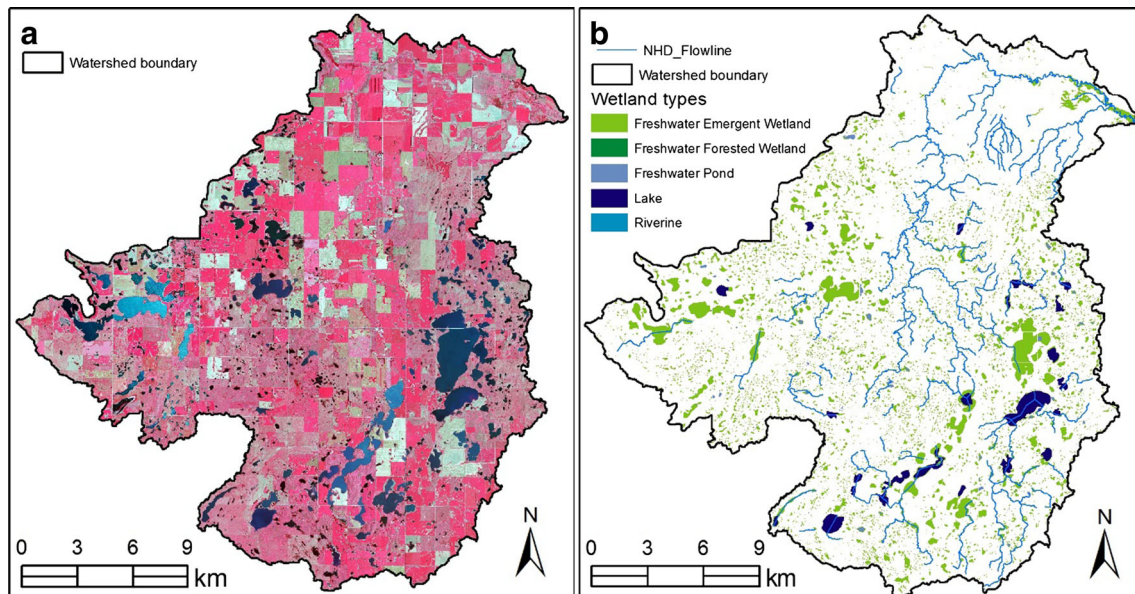


Fig. 3 Color-infrared aerial photographs and wetland inventory for the Little Pipestem Creek watershed: **a** false color composite of 1-m resolution aerial photographs (2012); **b** National Wetlands Inventory (NWI) data (1979–1984)

Table 3 Summary statistics of National Wetlands Inventory (NWI) data for our study area

Wetland type	Count	Min (m ²)	Max (m ²)	Median (m ²)	Sum (m ²)	Percentage
Freshwater emergent wetland	7,804	247	1,702,709	1,634	52,379,106	84.0 %
Freshwater forested/shrub wetland	17	1,129	8,559	2,326	57,037	0.1 %
Freshwater Pond	225	398	113,803	1,663	1,649,852	2.6 %
Lake	23	113,342	2,099,961	200,878	8,193,801	13.1 %
Riverine	22	1,153	18,579	2,684	96,327	0.2 %
Total (all polygons)	8,091	247	2,099,961	1,635	62,376,123	100.0 %

Methodology

Overview

Using the LiDAR-derived bare-earth DEM, we delineated potential wetland depressions and quantified their nested hierarchical structure with an innovative localized contour tree method. The LiDAR intensity imagery was used to extract existing waterbodies on the ground in late October 2011 when the LiDAR data were acquired. For the depression water storage modeling, we considered two types of depressional storage, the above-water volume and below-water volume. The below-water volume refers to the existing water volume stored in a wetland depression beneath the water surface, whereas the above-water volume is defined as the potential water volume a wetland depression can hold between the water surface and the spilling point. If a depression is completely dry without any existing water, the above-water volume refers to the storage volume between the lowest point in the basin (e.g., sink point) and the spilling point. By adding the computed above-water volume and the estimated below-water volume, we calculated the total storage volume for each individual wetland depression at different hierarchical levels, following the flowchart shown in Fig. 4.

Delineation of Wetland Depressions

The nested hierarchical structure of complex topographic depressions controls the dynamic filling, spilling, and merging hydrologic processes, as illustrated in Fig. 5a–c. We categorized topographic depressions into two groups: simple depressions and complex depressions. A simple depression is a depression that does not have any other depression nested inside, whereas a complex depression has at least two simple depressions nested inside. A large complex depression might also have some smaller complex depressions nested inside. The local minimum at the bottom of a depression is referred to as a sink point (see SP in Fig. 5a), and its elevation is less than or equal to that of its neighbors. As precipitation drains to a depression (or groundwater seeps in), the water surface in it will eventually be raised to a level at which water starts to spill from its perimeter. The lowest point on the depression perimeter is referred to as the spilling point (see SE in Fig. 5a), and

the elevation of the spilling point is referred to as the spill elevation (Wang and Liu 2006). If two or more adjacent simple depressions (i.e., 1st level depressions) share the same spill elevation, they will be merged and form a 2nd level complex depression. Similarly, further combination of 2nd level depressions forms even higher level depressions. Whenever two or more depressions merge, a higher depression level is created. The depression level represents the complexity of the nested hierarchical structure of a depression.

As shown in Fig. 5a–c, the complex depression **D** is a 2nd level depression, which has two 1st level simple depressions (**A** and **B**) nested inside. Similarly, the complex depression **E** is a 3rd level depression, in which three 1st level simple depressions (**A**, **B**, and **C**) and one 2nd level complex depression (**D**) are nested inside. The combination of the topological information about the nested hierarchical structure and the geometric attributes provides a comprehensive description and quantification of each individual surface depression across scales. The nested hierarchical structure of a complex depression can be represented as a depression tree graph (Fig. 5c). The nodes in the tree graph represent depressions, and the link between nodes represents the adjacency and containment relationships between depressions. In the depression contour tree, splitting and merging of nodes represent the change in topology. For example, when overland runoff flows into the simple depressions **A** and **B**, their water surfaces would gradually increase. When the water surfaces of simple depression

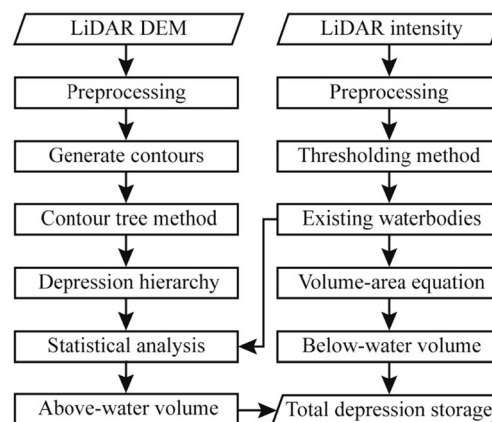
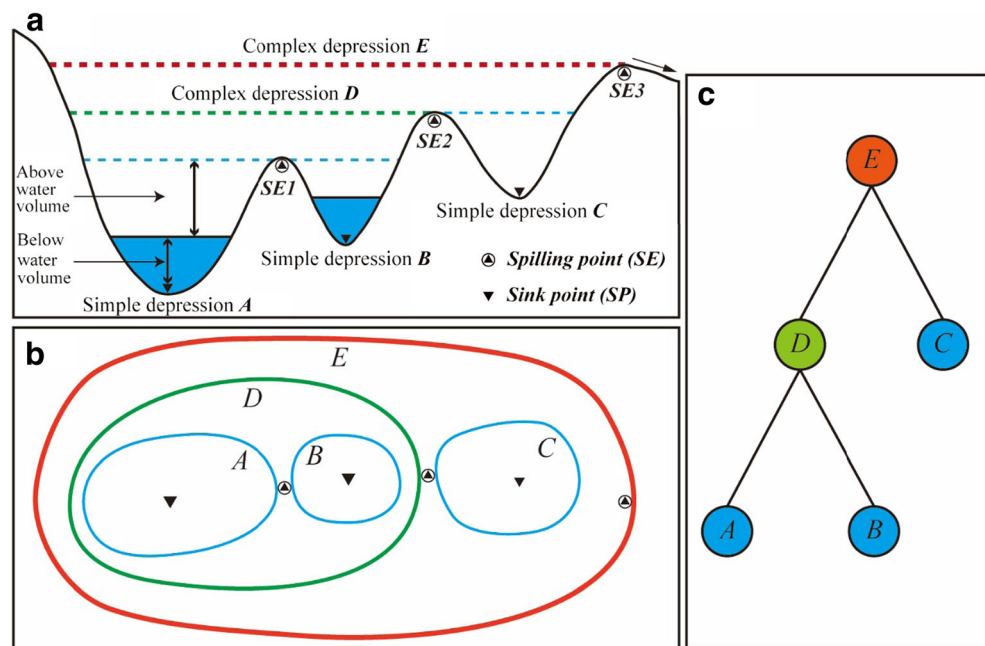


Fig. 4 Flowchart of our methods for delineating potential wetland depressions, quantifying depression hierarchical structure and estimating depression water storage volume

Fig. 5 Illustration of complex depression nested hierarchical structure: **a** profile view; **b** plan view; **c** depression tree representation; different color of nodes in the tree represent different portions of the complex depression basin in (a): blue (1st level), green (2nd level), red (3rd level)



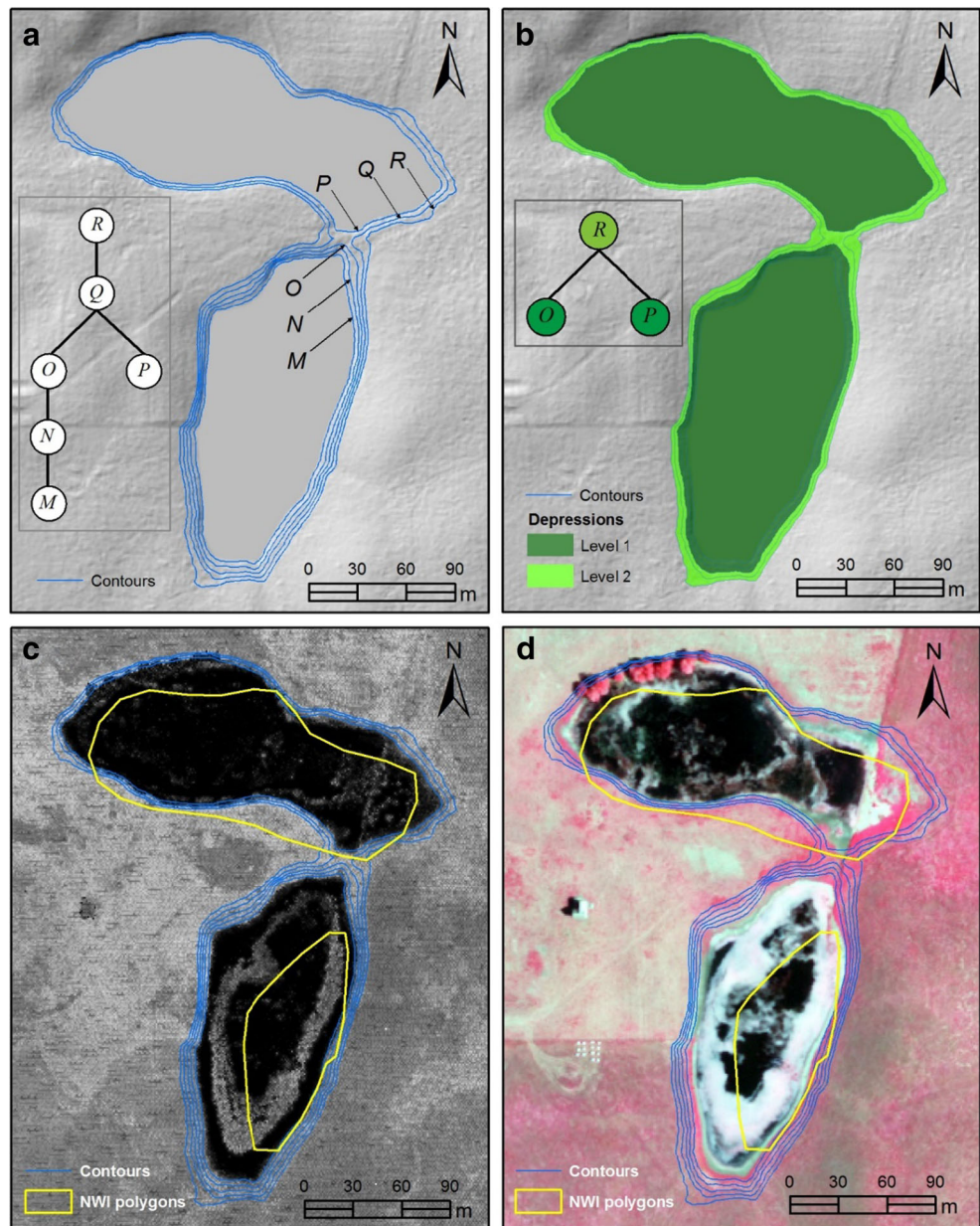
A and simple depression **B** reach to their spilling point **SE1**, these two adjacent depressions would merge to form a larger complex depression **D**, which is reflected by sibling nodes **A** and **B** joining at parent node **D** in the tree graph (Fig. 5c). When the water surface levels of simple depression **C** and complex depression **D** increase to above their spilling point **SE2**, these two depressions further combine to form an even more complex and larger surface depression **E**, which corresponds to the merge of nodes **C** and **D** at root node **E**. When the water surface level of complex depression **E** further increases to above the spilling point **SE3**, the water will spill into downstream basins. Clearly, the depression tree graph contains information about the nested hierarchical relationships among topographic depressions of different scales.

In a vector-based contour representation, a topographic depression is indicated by a series of concentric closed contours with the inner contours having lower elevation than their outer surrounding (Fig. 6a). The sink point is located inside the innermost closed contour. The outermost closed contour of the depression indicates the spatial extent (boundary) of the depression. The elevation of the outermost closed contour also approximates the spill elevation for the entire depression. Contours generated from high-resolution LiDAR DEMs often contain very jagged artifacts (Gonga-Saholiariliva et al. 2011). Therefore, it is a common practice to smooth the DEM before generating contours. The median or Gaussian smoothing filter is frequently used to remove data noise and suppress small artifact depressions without distorting the boundaries of true topographic depressions (Liu et al. 2010; Wu et al. 2014). The smoothed DEM is then used to generate contours. There are two key parameters for DEM contouring: the base contour and the contour interval. The base contour is typically set as zero

while the contour interval is chosen based on the topography of the mapped area and application needs. In this study, we set the contour interval as 20 cm, which was chosen based on the LiDAR vertical accuracy (15 cm) and consideration of computational time. DEM contouring generates two types of contours: closed contours and open contours. Closed contours are defined as contours which do not have starting or ending points while open contours are those with starting and ending points that intersect map edges at different locations (Lindsay 2004). In other words, a closed contour can form a loop while an open contour can not.

In the contour maps, depressions are represented as closed contours that are surrounded by other closed contours at a higher elevation. Consequently, only closed contours are kept for further analysis while open contours are eliminated. Topology within closed contours are then constructed. Specifically, each closed contour is attributed with its adjacent upward and outward contour and the corresponding contour elevation. To facilitate the algorithm for fast searching of depressions, we propose a new concept of “seed contours”, which are defined as closed contours that do not enclose any other contours. As shown in Fig. 6a, contours **M** and **P** are seed contours whereas contours **N**, **O**, **Q** and **R** are not. The depression seed contours serve as the starting point to search outwards for other associated closed depression contours, which are designated as the 1st level contours; these would be considered 1st level simple depressions (depending on subsequent analyses and topology). The topological relationships between depression contours can be represented by a contour tree. The concept of contour tree was first proposed by Kweon and Kanade (1994) for representing the spatial relations of contour lines where contours are mapped as nodes and

Fig. 6 Illustration of localized contour tree method for depression delineation. The contour interval is 20 cm; **a** contour tree representation. The letters on the contour surface correspond to the nodes in the contour tree graph; **b** depression tree (simplified contour tree) representation; **c** closed contours and National Wetlands Inventory (NWI) polygons overlaid on LiDAR intensity imagery (2011); **d** closed contours and National Wetlands Inventory (NWI) polygons overlaid on color-infrared aerial photographs (2012)



interstitial spaces as links. Similar to the depression tree graph shown in Fig. 5c, the nodes in the contour tree graph represent contours, and the link between nodes represents the adjacency and containment relationships between contours. In the contour tree, splitting and merging of nodes represent the change in topology. As shown in contour tree graph in Fig. 6a, contour **N** encloses the seed contour **M** (1st level), and there is no topological change between them. Therefore, contour **N** is also determined as the 1st level contour, the same level as the depression seed contour **M**. Similarly, contour **O** is also determined as 1st level contour, since there is no topological change between contours **N** and **O**. With the water level further increasing another 20 cm (the contour interval in our study), the contours **O** and **P** would merge to form a larger

depression with a 2nd level contour **Q**. This iterative procedure continues until all the depression seed contours and their outward closed contours are processed and depression levels are determined accordingly. In the case example shown in Fig. 6a, the most upward and outward contour **R** would be determined as a 2nd level depression contour, which represents the boundary of the complex depression.

From the perspective of graph theory, the hierarchical relationships of nested depressions inside a complex depression also constitutes a tree. The most outward contour of the complex depression is the root of the tree, the directed links between two adjacent contours are the edges of the tree, and seed contours are the leaf nodes of the tree. We employ the depression seed contours as the starting point to search upwards and

outwards to minimize search time for establishing the tree or forest of trees. Compared to the global contour tree method (Wu 2011), the proposed localized contour tree method is more effective and computationally efficient. Instead of creating a single global tree for the entire area, the localized contour tree algorithm constructs a forest of trees. The elevation boundary of a surface depression corresponds to a closed contour with the same elevation as its spilling point, which is referred to as the spilling contour in this study. The spilling point of the depression is located on its spilling contour. Therefore, the task of topographic depression detection becomes the identification of spilling contours. To explicitly represent the nested hierarchical structure of a complex depression, the local contour tree is simplified by removing the nodes that do not correspond to spilling contours. After simplification, the six-node contour depression tree in Fig. 6a is reduced to a smaller and compact complex depression tree with only three nodes (Fig. 6b). The complexity level of a complex depression can be measured by the number of nodes passing through the longest path from the root node to the leaf nodes. Traversing the depression tree top-down simulates the splitting of a large complex depression into smaller lower level depressions when water level decreases, while traversing the depression tree bottom-up emulates the merging of smaller lower level depressions into larger and more complex depressions when water level increases. A complex depression may have more than one first level simple depressions embedded within it, depending on the selection of contour intervals and the elevation difference between the lowest point in the depression and the spill contour elevation. Each depression tree represents one complex depression, and the number of trees in the forest represent the number of complex depressions for the entire area.

Identification of Existing Waterbodies

After delineating wetland depressions from the LiDAR DEM and quantifying the complexity of their nested hierarchical structure using the localized contour tree method, we determined the presence of standing (antecedent) water in each individual depression to contrast a LiDAR-based assessment with existing area and volume assessments. We applied the following methodology to quantify the maximum volume of water stored in these systems before the spill elevation was reached, applying an area-to-volume algorithm to quantify below-water storage. Wetlands with standing water were characterized with low LiDAR intensity values (i.e., were darker than the surrounding areas), while other land cover types (e.g., cultivated crops, upland grassland) had higher intensity values and were lighter in color. Simple thresholding techniques have been used in previous studies to extract standing waterbodies in LiDAR intensity imagery (Lang and McCarty 2009; Huang et al. 2011b). The 1-m gridded LiDAR intensity imagery for our study area was smoothed using a 3×3 median filter. The

filtered intensity image was then used to separate water and non-water pixels. We set a threshold value to separate water and non-water pixels by examining typical waterbodies. The threshold was set at an intensity value of 30 based on examination of the intensity histogram and visual inspection of typical waterbodies in the LiDAR intensity imagery. Areas with intensity values between 0 and 30 were mapped as waterbodies while areas with intensity values between 31 and 255 were mapped as non-water. More detailed description on water pixel classification using LiDAR intensity has been provided by (Huang et al. 2014).

Estimating Water Storage Volume

After completion of the identification of potential wetland depressions and delimiting and quantifying depression complexity levels (e.g., Fig. 5c), various geometric attributes of depressions can be computed for all depression contour levels, including simple and complex depression surface area, perimeter, maximum depth, mean depth, and depression storage, etc. The above-water volume (V_{AW}) (e.g., see Fig. 5a) for each simple depression that comprises a complex depression (as applicable) can be calculated based on statistical analysis of LiDAR DEM cells enclosed by the depression boundary (or spilling) contour

$$V_{AW} = (Z \times C - S) \times R^2 \quad (1)$$

where Z = elevation of the depression boundary contour; C = number of cells enclosed by the depression boundary contour; S = summation of elevation values of all cells enclosed by the depression contour; and R = pixel resolution of the DEM grid. The maximum depression storage for the entire complex depression area is the summation of depression storage from all simple depressions. We further calculated V_{AW} for all depressions that were without any standing water to contrast LiDAR-based volume assessments to area-to-volume equations.

Since the near-infrared LiDAR sensors generally could not penetrate water, the depression morphology beneath the water surface could not be derived from LiDAR data. Therefore, it is not possible to calculate the exact storage volume of an existing waterbody. However, numerous studies have showed that there is a strong statistical relationship between storage volume (V) and surface area (A) in a topographic depression (Ullah and Dickinson 1979b; Hayashi and Van der Kamp 2000; Gleason et al. 2007; Minke et al. 2010; Le and Kumar 2014). Gleason et al. (2007) developed a general area-to-volume equation (Eq. 2) relating the volume (V) and wetted area (A) to estimate water storage in pothole wetlands in the Glaciated Plains physiographic region.

$$V = 0.25 \times A^{1.4742} \quad (2)$$

where A is the measured surface area in hectares and V is the predicted storage volume in hectare-meters. Since our study area is located in the Glaciated Plains, we adopted and modified Eqs. (2) to (3) by transforming the storage volume unit from hectare-meters to cubic meters:

$$\begin{aligned} V_{BW} &= 0.25 \times \left(A / 10,000 \right)^{1.4742} \times 10,000 \\ &= 0.00317 \times A^{1.4742} \end{aligned} \quad (3)$$

where A is the water surface area in m^2 and V_{BW} is the predicted existing below-water storage volume in m^3 . By adding the LiDAR-computed above-water volumes (V_{AW}) and the estimated below-water volumes (V_{BW}), we calculated the total storage volume (V_{TW}) for each wetland depression (simple depressions or complex depressions) at different levels (Eq. 4).

$$V_{TW} = V_{AW} + V_{BW} \quad (4)$$

Equation (4) combines the maximum potential storage from the lowest point of the contour polygon that is above water (and thus calculated through LiDAR analyses of simple or complex depressions) to the spill elevation plus the calculated volume of water estimated to exist below the wetted area of the wetland depression (as applicable).

Results

We applied our approach to the Little Pipestem Creek watershed. After smoothing the 1-m LiDAR-derived bare-earth DEM using a 3×3 median filter, we generated the vector contour representation by setting the base contour of each depression to be zero meters and the contour interval to be 20 cm. The localized contour tree method was then applied to contours to identify topographic depressions in the study area (Fig. 7). In total, 12,402 depressions were detected and characterized, of which 11,301 were 1st-level simple depressions, and 1,101 were multi-level (e.g., >1st level) complex depressions. The greatest complexity was found in an eight-level system. For each surface depression (simple depression or complex depressions), geometric and topological properties were computed.

Using the LiDAR intensity data, we identified 3,269 out of 12,402 wetland depressions with standing water. The total water surface area was approximately 5,350 ha, with an average size of 2.04 ha and a median size of 0.182 ha, which is slightly larger than the median size (0.164 ha) of NWI polygons in the study area. Using the V_{BW} equation (Eq. 3), we estimated that these existing waterbodies contained approximately 104.7 million m^3 of water. We also contrasted the LiDAR-based storage potential (i.e., Eq. 1) with the area-to-

volume relationship based storage potential equations (i.e., Eq. 3) for the remaining 9,133 dry depressions, which were comprised of 8,676 (95.0 %) simple depressions and 457 (5 %) complex depressions (Fig. 8).

Among the dry depressions, 8,643 (88 %) were less than 0.20 ha in size. The total surface area of all dry depressions was approximately 1,253 ha. The total LiDAR-computed volume and area-to-volume equation predicted volume were 3.87 and 3.35 million m^3 , respectively. Overall, the storage volumes using the area-to-volume relationship established in Eq. (3) tended to underestimate the LiDAR-computed storage volumes using Eq. (1) in our study area, and no distinct pattern was found for measured storage for simple or complex depressions (see Fig. 8). Nevertheless, the area-to-volume equation developed by Gleason et al. (2007) provides a reasonable estimate of full depression storage volume when high-resolution topographic data is not available for precisely calculating the storage volume. Since the area-to-volume equation developed for the Glaciated Plains by Gleason et al. (2007) underestimated the storage volume for wetland depressions in our study area, we fitted a new power function curve to these dry depressions (Eq. 5).

$$V = 0.01725 \times A^{1.30086} \quad (5)$$

The fitted power function curve is slightly above the area-to-volume estimated volume, providing a better area-to-volume model for estimating storage volume for wetland depressions in the watershed.

Discussion

Our localized contour tree method is fundamentally different from the previous raster-based methods for topographic depression detection, which use the priority-flood algorithm and its variants to create a hydrologically connected surface by flooding DEMs inwards from their edges (Lindsay and Creed 2006; Wang and Liu 2006; Barnes et al. 2014). The depressions are then derived by subtracting the original DEM from the depression-filled DEM. These raster-based methods assume that the surface is fully flooded and ignore the nested hierarchical structure within depressions. On the contrary, our method for topographic depression detection is a vector-based approach that does not make the fully-flooded assumption. We treated the topographic depression detection problem as the identification of a set of concentric contours with an increasing elevation outward, represented by a contour tree. Localized contour tree construction and search algorithms make our method computationally efficient and fast. The detection results for topographic depression are likely to be consistent with human interpretation results.

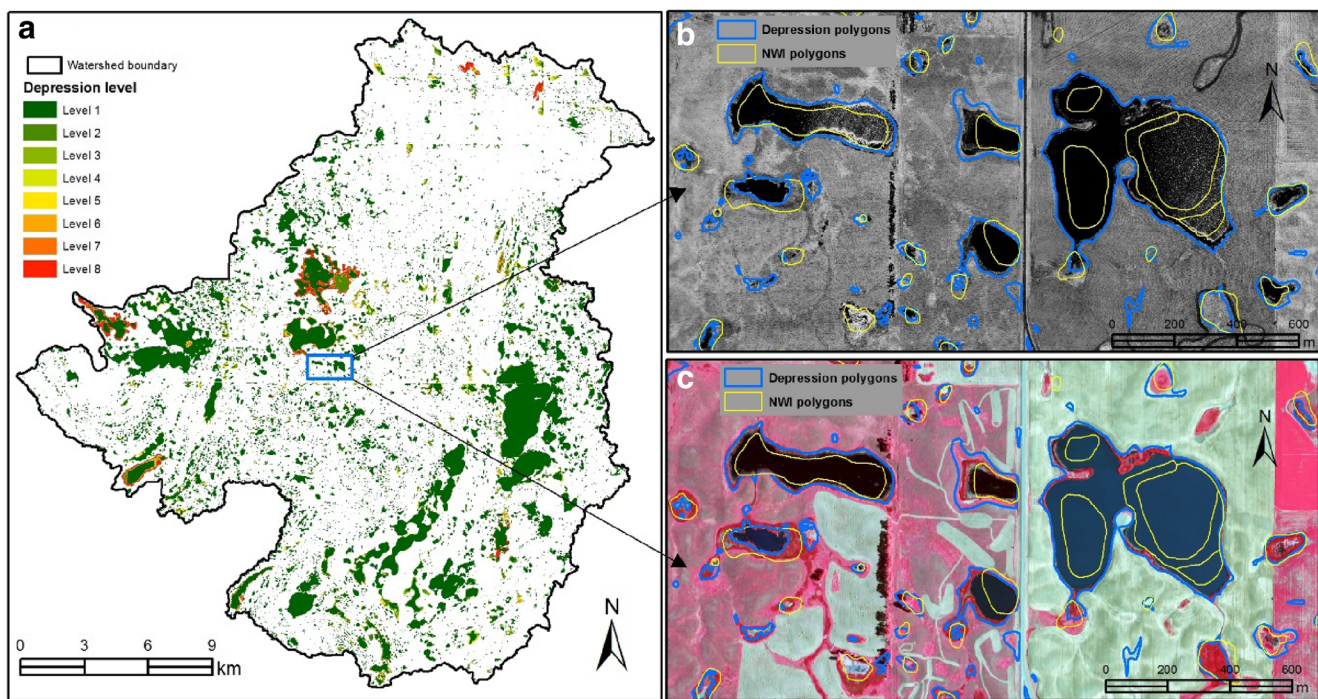


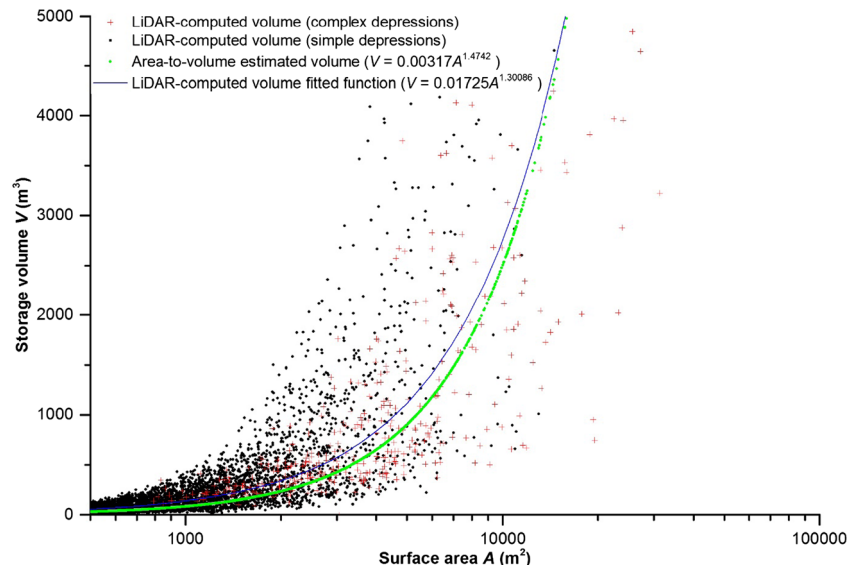
Fig. 7 Depression delineation and quantification for Little Pipestem Creek watershed: **a** spatial distribution of detected depressions; **b** depression boundaries and National Wetlands Inventory (NWI) polygons

overlaid on the LiDAR intensity imagery (2011); **c** depression boundaries and National Wetlands Inventory (NWI) polygons overlaid on the false-color composite of aerial photographs (2012)

The reliability and accuracy of the topographic depressions detected by our localized contour tree method may be affected by a number of factors. The spatial resolution and vertical accuracy of LiDAR-derived bare-earth DEM largely determines the minimum size and depth of depressions that can be reliably detected by our contour tree method. Generally, the detection and delineation of smaller and shallower topographic depressions needs higher spatial resolution and vertical accuracy of LiDAR data. The LiDAR DEM for our study area has a 1-m spatial resolution with a vertical accuracy of 15 cm. It should be

able to detect a depression with a diameter of 2 m and a depth of 30 cm according to the Nyquist-Shannon sampling theorem (Blaschke 2010). Since our method is based on the contour representation of depressions, the selection of the base contour line and particularly the contour interval would also affect the depression detection result. The larger the contour interval, the fewer contour lines generated and the less computation time needed to detect depressions (and vice versa). The contour interval chosen to generate contours for our study area was 20 cm. Consequently, our localized contour tree might not detect some

Fig. 8 Comparisons of depression area-volume relationships between LiDAR-computed and area-to-volume equation predicted models



shallow depressions whose depths are less than the chosen contour interval (20 cm), as these depressions might be absent from the contour maps even when these features actually exist in the landscape. This is the intrinsic limitation of DEM contouring. The number of artifact depressions resulted from LiDAR DEM error could be effectively reduced by setting appropriate thresholds of surface area and depth of depressions. As recommended by Li et al. (2011), soil and climate conditions of the site, the process of interest and the scope of the study all need to be taken into account when making the decision on selecting appropriate minimum depression area and depth thresholds.

It is also important to note the ideal conditions for LiDAR data collection is leaf-off and dry antecedent conditions for wetland depression analyses. LiDAR generally cannot penetrate water, meaning that the basin morphology of inundated depressions could not be captured by LiDAR data. Therefore, it is not possible to calculate the exact water volume under the existing water surface. The LiDAR used in our study were collected during late October to early November in 2011, which was after vegetation senescence. However, the depressions appear to be wetter than that in the summer season, as evidenced from water surface comparisons between the LiDAR intensity imagery (2011) and aerial photographs (2012) in Fig. 6c and d, as well as in Fig. 7b and c.

As mentioned earlier, the National Wetlands Inventory (NWI) data that have been widely used for studying wetlands across the PPR are considerably out of date, as they were manually interpreted from 1979 to 1984 aerial photographs. There were substantial position errors associated with the NWI polygons in our study area (see examples in Figs. 6 and 7). In addition, the NWI data dramatically underestimated the areal extent of current wetland depressions, especially for those large waterbodies. There is a compelling need to update the wetlands inventory in the PPR.

Conclusions

Reliable and up-to-date wetland extent is essential for improving conservation and management of wetlands and flood mitigation efforts. In this study, we developed a new approach for delineating wetland depressions, quantifying their nested hierarchical structure, and estimating depression water storage volume using LiDAR DEM and LiDAR intensity imagery. Although information presented in this study is specific to the Little Pipestem Creek watershed, the proposed method is applicable to other portions of the Prairie Pothole Region, as well as other areas with sufficiently high resolution topographic data. With the increasing availability and high-resolution LiDAR data and aerial photographs in the PPR, the proposed method is very promising for monitoring and updating wetland extent and estimating water storage capability.

This research contributes to digital terrain analysis by providing a new framework for identifying topographic depressions for hydrologic analysis and modelling. Specifically, this research takes into account dynamic hydrological processes through an innovative localized contour tree method to identify surface depressions and quantify both their simple and complex topological relationships. The hierarchical structure and geometric properties of depressions derived from our method could, we hope, lead to more realistic and accurate hydrologic analysis.

Acknowledgments We are grateful to the State of North Dakota's GIS Hub, which provided LiDAR data and aerial photographs to support this research. We would also like to thank two anonymous reviewers. Their comments and suggestions have been very helpful for improving the quality of this paper. This paper has been reviewed in accordance with the U.S. Environmental Protection Agency's peer and administrative review policies and approved for publication. Mention of trade names or commercial products does not constitute endorsement or recommendation for use. Statements in this publication reflect the authors' professional views and opinions and should not be construed to represent any determination or policy of the U.S. Environmental Protection Agency.

Appendix

The proposed contour tree method for depression identification has been implemented as an ArcGIS toolbox – Depression Identification Analyst, which will be freely available upon request. The Depression Identification Tool asks the user to provide a single input, the LiDAR DEM, and then executes the aforementioned procedures with user-specified parameters (base contour, contour interval, minimum depression area, minimum depression depth, etc.) automatically to create depression polygons at different hierarchical levels. All depression results can be saved as ESRI Shapefile or Geodatabase format.

References

- Barnes R, Lehman C, Mulla D (2014) Priority-flood: an optimal depression-filling and watershed-labeling algorithm for digital elevation models. *Computers & Geosciences* 62:117–127. doi:[10.1016/j.cageo.2013.04.024](https://doi.org/10.1016/j.cageo.2013.04.024)
- Blaschke T (2010) Object based image analysis for remote sensing. *ISPRS Journal of Photogrammetry and Remote Sensing* 65:2–16. doi:[10.1016/j.isprsjprs.2009.06.004](https://doi.org/10.1016/j.isprsjprs.2009.06.004)
- Cowardin LM, Carter V, Golet FC, LaRoe ET (1979) Classification of wetlands and deepwater habitats of the United States. U.S. Department of the Interior, Fish and Wildlife Service, Washington, 131 pp
- Dahl TE (1990) Wetlands losses in the United States, 1780's to 1980's. Report to the congress. U.S. Department of the Interior, Fish and Wildlife Service, Washington, 13 pp
- Dahl TE (2014) Status and trends of prairie wetlands in the United States 1997 to 2009. U.S. Department of the Interior, Fish and Wildlife Service, Ecological Services, Washington, 67 pp

- Ehsanzadeh E, Spence C, van der Kamp G, McConkey B (2012) On the behaviour of dynamic contributing areas and flood frequency curves in North American Prairie watersheds. *Journal of Hydrology* 414–415:364–373. doi:[10.1016/j.jhydrol.2011.11.007](https://doi.org/10.1016/j.jhydrol.2011.11.007)
- Euliss NH et al (2004) The wetland continuum: a conceptual framework for interpreting biological studies. *Wetlands* 24:448–458
- Gleason RA, Tangen BA, Laubhan MK, Kermes KE, Euliss NH Jr (2007) Estimating water storage capacity of existing and potentially restorable wetland depressions in a subbasin of the Red River of the North. U.S. Geological Survey Open-File Report 2007–1159. 36pp
- Gonga-Saholiariliva N, Gunnell Y, Petit C, Mering C (2011) Techniques for quantifying the accuracy of gridded elevation models and for mapping uncertainty in digital terrain analysis. *Progress in Physical Geography* 35:739–764
- Haag KH, Lee TM, Herndon DC, County P, Water TB (2005) Bathymetry and vegetation in isolated marsh and cypress wetlands in the northern Tampa Bay area, 2000–2004. U.S. Geological Survey Scientific Investigations Report 2005–5109. 49 pp
- Hayashi M, Van der Kamp G (2000) Simple equations to represent the volume-area-depth relations of shallow wetlands in small topographic depressions. *Journal of Hydrology* 237:74–85
- Huang S, Dahal D, Young C, Chander G, Liu S (2011a) Integration of Palmer Drought Severity Index and remote sensing data to simulate wetland water surface from 1910 to 2009 in Cottonwood Lake area, North Dakota. *Remote Sensing of Environment* 115:3377–3389
- Huang S, Young C, Feng M, Heidemann K, Cushing M, Mushet DM, Liu S (2011b) Demonstration of a conceptual model for using LiDAR to improve the estimation of floodwater mitigation potential of Prairie Pothole Region wetlands. *Journal of Hydrology* 405:417–426
- Huang C, Peng Y, Lang M, Yeo IY, McCarty G (2014) Wetland inundation mapping and change monitoring using landsat and airborne LiDAR data. *Remote Sensing of Environment* 141:231–242
- Jin S, Yang L, Danielson P, Homer C, Fry J, Xian G (2013) A comprehensive change detection method for updating the national land cover database to circa 2011. *Remote Sensing of Environment* 132:159–175
- Johnson RR, Oslund FT, Hertel DR (2008) The past, present, and future of prairie potholes in the United States. *Journal of Soil and Water Conservation* 63:84A–87A
- Johnston CA (2013) Wetland losses due to row crop expansion in the dakota prairie pothole region. *Wetlands* 33:175–182. doi:[10.1007/s13157-012-0365-x](https://doi.org/10.1007/s13157-012-0365-x)
- Kweon IS, Kanade T (1994) Extracting topographic terrain features from elevation maps. *CVGIP: Image Understanding* 59:171–182. doi:[10.1006/cium.1994.1011](https://doi.org/10.1006/cium.1994.1011)
- Lane C, D'Amico E (2010) Calculating the ecosystem service of water storage in isolated wetlands using LiDAR in north central Florida, USA. *Wetlands* 30:967–977. doi:[10.1007/s13157-010-0085-z](https://doi.org/10.1007/s13157-010-0085-z)
- Lang M, McCarty G (2009) LiDAR intensity for improved detection of inundation below the forest canopy. *Wetlands* 29:1166–1178. doi:[10.1672/08-197.1](https://doi.org/10.1672/08-197.1)
- Le PV, Kumar P (2014) Power law scaling of topographic depressions and their hydrologic connectivity. *Geophysical Research Letters* 41: 1553–1559
- Li S, MacMillan RA, Lobb DA, McConkey BG, Moulin A, Fraser WR (2011) LiDAR DEM error analyses and topographic depression identification in a hummocky landscape in the prairie region of Canada. *Geomorphology* 129:263–275. doi:[10.1016/j.geomorph.2011.02.020](https://doi.org/10.1016/j.geomorph.2011.02.020)
- Lindsay JB (2004) Coping with topographic depression in digital terrain analysis. PhD thesis, University of Western Ontario
- Lindsay JB, Creed IF (2006) Distinguishing actual and artefact depressions in digital elevation data. *Computers and Geosciences* 32: 1192–1204. doi:[10.1016/j.cageo.2005.11.002](https://doi.org/10.1016/j.cageo.2005.11.002)
- Liu H, Wang L, Sherman D, Gao Y, Wu Q (2010) An object-based conceptual framework and computational method for representing and analyzing coastal morphological changes. *International Journal of Geographical Information Science* 24:1015–1041. doi:[10.1080/13658810903270569](https://doi.org/10.1080/13658810903270569)
- McCauley L, Anteau M (2014) Generating nested wetland catchments with readily-available digital elevation data may improve evaluations of land-use change on wetlands. *Wetlands* 1–10. doi:[10.1007/s13157-014-0571-9](https://doi.org/10.1007/s13157-014-0571-9)
- Miller MW, Nudds TD (1996) Prairie landscape change and flooding in the Mississippi River Valley. *Conservation Biology* 10:847–853
- Minke A, Westbrook C, van der Kamp G (2010) Simplified volume-area-depth method for estimating water storage of prairie potholes. *Wetlands* 30:541–551. doi:[10.1007/s13157-010-0044-8](https://doi.org/10.1007/s13157-010-0044-8)
- Ouyang ZT, Becker R, Shaver W, Chen JQ (2014) Evaluating the sensitivity of wetlands to climate change with remote sensing techniques. *Hydrological Processes* 28:1703–1712. doi:[10.1002/hyp.9685](https://doi.org/10.1002/hyp.9685)
- Shaw DA, Pietroniro A, Martz L (2013) Topographic analysis for the prairie pothole region of Western Canada. *Hydrological Processes* 27:3105–3114
- Shook K, Pomeroy J (2012) Changes in the hydrological character of rainfall on the Canadian prairies. *Hydrological Processes* 26:1752–1766
- Sloan CE (1972) Ground-water hydrology of prairie potholes in North Dakota. Professional paper 585-c. U.S. Government Printing Office, Washington
- Tiner RW (1997) NWI maps: what they tell us. *National Wetlands Newsletter* 19:7–12
- Todhunter PE, Rundquist BC (2004) Terminal lake flooding and wetland expansion in Nelson County, North Dakota. *Physical Geography* 25: 68–85
- Townsend-Small A, Pataki DE, Liu H, Li Z, Wu Q, Thomas B (2013) Increasing summer river discharge in southern California, USA, linked to urbanization. *Geophysical Research Letters* 40:4643–4647. doi:[10.1002/grl.50921](https://doi.org/10.1002/grl.50921)
- Ullah W, Dickinson WT (1979a) Quantitative description of depression storage using a digital surface model: I. Determination of depression storage. *Journal of Hydrology* 42:63–75. doi:[10.1016/0022-1694\(79\)90006-4](https://doi.org/10.1016/0022-1694(79)90006-4)
- Ullah W, Dickinson WT (1979b) Quantitative description of depression storage using a digital surface model: II. Characteristics of surface depressions. *Journal of Hydrology* 42:77–90. doi:[10.1016/0022-1694\(79\)90007-6](https://doi.org/10.1016/0022-1694(79)90007-6)
- Wang L, Liu H (2006) An efficient method for identifying and filling surface depressions in digital elevation models for hydrologic analysis and modelling. *International Journal of Geographical Information Science* 20:193–213
- Winter TC (1989) Hydrologic studies of wetlands in the northern prairie. In: Van der Valk AG (ed) Northern prairie wetlands. Iowa State University Press, Ames, pp 16–54
- Winter TC, Rosenberry DO (1995) The interaction of ground water with prairie pothole wetlands in the Cottonwood Lake area, east-central North Dakota, 1979–1990. *Wetlands* 15:193–211
- Wu Q (2011) Object-oriented representation and analysis of coastal changes for hurricane-induced damage assessment. Electronic Thesis or Dissertation, University of Cincinnati
- Wu Q, Lane C, Liu H (2014) An effective method for detecting potential woodland vernal pools using high-resolution LiDAR data and aerial imagery. *Remote Sensing* 6:11444–11467. doi:[10.3390/rs61111444](https://doi.org/10.3390/rs61111444)
- Wu B, Yu B, Huang C, Wu Q, Wu J (2016) Automated extraction of ground surface along urban roads from mobile laser scanning point clouds. *Remote Sensing Letters* 7:170–179. doi:[10.1080/2150704X.2015.1117156](https://doi.org/10.1080/2150704X.2015.1117156)
- Yang J, Chu X (2013) Quantification of the spatio-temporal variations in hydrologic connectivity of small-scale topographic surfaces under various rainfall conditions. *Journal of Hydrology* 505:65–77. doi:[10.1016/j.jhydrol.2013.09.013](https://doi.org/10.1016/j.jhydrol.2013.09.013)